RSC Advances

PAPER

View Article Online
View Journal | View Issue

Cite this: *RSC Adv.*, 2020, **10**, 32400

Effect of triblock copolymers on crystal growth and the photocatalytic activity of anatase TiO_2 single crystals

Yeshuo Dong *[a] and Fanjun Meng[b]

In order to evaluate the effect of a triblock copolymer on the growth of TiO_2 crystals, anatase TiO_2 crystals with different morphologies and structures were synthesized by controlling the content and type of triblock copolymer in the solvothermal route. The resulting samples were characterized by XRD, XPS, SEM, TEM and EDX. The characterization results show that hydrofluoric acid can promote the formation of highly active (001) facets by the formation of a Ti–F bond. The triblock copolymers (P123 and F127) refine the surface structure of polycrystalline spherical TiO_2 and make the crystal surface homogeneous and smooth. Moreover, P123 causes the agglomeration effect and hinders the recrystallization process of anatase TiO_2 single crystals, and this will lead to corrosion of the crystal facets. Meanwhile, F127 destroys crystal formation and hinders crystal growth due to its special micelle structure. In addition, research on the photocatalytic activity proposed that the integrity of the (001) and (101) facets was a critical factor in the photocatalytic reaction. The resultant anatase TiO_2 single crystals could produce more hydroxyl radicals (•OH) in the photocatalytic system, which exhibited remarkable photocatalytic performance for the degradation of three types of dye.

Received 8th July 2020
Accepted 20th August 2020

DOI: 10.1039/d0ra05965j

rsc.li/rsc-advances

1. Introduction

Over the past decade, due to a semiconductor crystal with a specific structure having many inherent characteristics of a crystal facet, research on the atomic structure and crystal lattice of the semiconductor crystal with a specific crystal facet has attracted a lot of attention from researchers.[1–5] Moreover, the equilibrium and steady-state chemical properties of the crystal facet are crucial for the synthesis of highly active catalytic materials.[6,7] Titania, as a semiconductor crystal, has been widely used in the fields of environmental pollution control, H_2-production, solar cells, photovoltaic power generation and sensor design.[8–11] However, the realization of these applications usually depends on the crystal structure, the activity of the crystal facet and the specific micromorphology of TiO_2.[12–14] Therefore, research on the crystal structure and crystal facet characteristics of TiO_2 has been widely carried out,[15,16] and many TiO_2 materials with different structures have been successfully synthesized, such as nanoparticles, porous materials, multi-element composites, flakes, spheres and tubes.[9,17,18]

With the improvement of the synthetic technology and the in-depth study of the TiO_2 crystal structure, both theoretical and experimental studies found that the (001) facets in the equilibrium and stable states had higher photocatalytic activities.[19,20] In 2008, the anatase TiO_2 single crystals were successfully synthesized with a large percentage (47%) of reactive (001) facets.[21] In addition, this research stated that the surface energy of the crystals could be effectively decreased using hydrofluoric acid as a morphology controlling agent with the formation of a Ti–F bond. Following this, various kinds of TiO_2 single crystals marked by (001) facet exposure, such as sheet TiO_2 single crystals, nano TiO_2 single crystals and mesoporous TiO_2 single crystals, were synthesized by adding different crystal morphology controlling agents and growth controlling agents.[22–24] For growth controlling agents in particular, they are very important for the adjustment of grain size, crystal surface characteristics and crystal dispersion in the synthetic process.[25,26] Generally, the commonly used crystal growth control agents are surfactants, silica templates, and dispersants.[27,28] In addition, with further study of the crystal growth mechanism, more and more additives have been found and have been proved to affect the growth rate and morphology of the crystals.[29,30]

In recent years, triblock copolymers (polyoxyethylene–polyoxypropylene–polyoxyethylene: PEO–PPO–PEO) have been widely used as blending compatibilizers and interface modifiers in biomedical, architectural, chemical, and other, fields.[31,32] As very important water-soluble substances, triblock copolymers spontaneously form micelles in aqueous solution. The cores and the shells of the micelles were mainly composed of PPO and PEO, respectively, and, as growth regulators of inorganic crystals, triblock copolymers have been successfully applied to effectively control the morphology and structure of inorganic particles.[33] Some studies have proven that triblock copolymers can be used as

[a]*School of Environmental and Municipal Engineering, Qingdao University of Technology, Qingdao, 266033, China. E-mail: dysh_1127@aliyun.com*
[b]*College of Chemistry, Chemical Engineering and Materials Science, Shandong Normal University, Jinan, 250014, China*

an auxiliary pore-forming agent and as a template to accelerate hydroxylation and substitution of inorganic crystals in a hydrothermal environment.[34] Moreover, other studies have shown that triblock copolymers can also promote the nucleation and self-assembly processes.[35] For example, in the crystallization processes of calcium carbonate and barium sulfate, triblock copolymers are essential control agents of crystal growth.[36] For the synthesis of TiO_2 crystals, the current research into triblock copolymers on crystal growth is not sufficient.[37] The role of triblock copolymers in the hydrothermal synthesis process of TiO_2 crystals still needs to be further explored.

Based on the above reasons, P123 and F127 (triblock copolymers) were chosen as the crystal growth controlling agents in this work. As is well-known, P123 and F127 are common triblock copolymers, and the critical micelle concentration (cmc) of P123 is much lower than that of F127. At the same temperature, the aggregation number of the P123 micelles is almost three times that of the F127 micelles, and this means that the volumes of the P123 micelles are larger. In addition, the P123 micelles are composed of a hydrophobic PPO core and a short block hydrophilic PEO shell. Compared with P123, the F127 micelles have a smaller volume and a longer PEO block, which makes the micelle shell very thick and have better dispersion in water. Therefore, the interaction between the F127 micelles and water is stronger. The anatase TiO_2 crystals with different morphologies and structures were synthesized under the action of hydrofluoric acid and the triblock copolymers.[38] The effects of P123 and F127 on the growth of the TiO_2 crystals were evaluated by the characterization of their microstructures and morphologies. This study provides a reference for the excellent synthesis of anatase TiO_2 single crystals. Moreover, in order to evaluate the photocatalytic performances of the resultant TiO_2 photocatalysts, the photocatalytic properties for the heterogeneous photocatalytic reaction were monitored by the terephthalic acid method and photocatalytic degradation of three types of dye.

2. Experimental methods

2.1 Synthesis and characterization of materials

Anatase TiO_2 crystals with different morphologies were synthesized through a solvothermal method. In this work, hydrofluoric acid and the triblock copolymers were used as the crystal facet controlling agent and growth controlling agents, respectively. Titanium tetrafluoride (TiF_4; Sigma-Aldrich) was dissolved in hydrochloric acid solution under vigorous stirring to give a concentration of 0.01 mol L^{-1} and a pH value of 1.5. TiF_4 solution (0.01 mol L^{-1}), hydrofluoric acid (HF, 40 wt%) and the triblock copolymers (P123 and F127) were added into a 100 mL Teflon-lined stainless-steel autoclave. The autoclave was kept at 160 °C for 4–12 h in an electric oven. After the reaction, the anatase TiO_2 crystals were harvested by centrifugation, washed twice with deionized water, and then dried at 120 °C for 2 h.[29,39] The surface fluorine molecules of the samples were removed through a heat treatment process at 500 °C for 90 min. Then, the samples were cooled to room temperature for further activity experiments and characterizations.

The morphologies and structures of the as-synthesized anatase TiO_2 crystals were investigated by X-ray spectroscopy (XRD, Bruker D8 Advance), transmission electron microscopy (TEM, JEM-2100, Japan) and scanning electron microscopy (SEM, JEOLJSM6400F) equipped with an EDX. Prior to TEM analysis, powdered samples were dispersed onto a carbon-coated copper grid. N_2-adsorption and desorption of the samples were measured by a specific surface area analyzer (F-Sorb 3400). Specific surface areas were calculated according to the Brunauer–Emmett–Teller (BET) equation. X-ray photoelectron spectroscopy (XPS) measurements were carried out using a Kratos AXIS Ultra DLD XPS system. All the binding energies were referenced to the C 1s peak (285.0 eV) arising from an adventitious carbon atom.

2.2 Photocatalytic measurements

2.2.1. Hydroxyl radical (˙OH) measurement. As is well-known, the terephthalic acid method is usually used to determine the presence of hydroxyl radicals (˙OH).[40,41] Terephthalic acid (TA) is used as a fluorescence probe because it can react with ˙OH in basic solution to generate 2-hydroxy terephthalic acid (TAOH), which emits a unique fluorescence signal with a spectrum peak around 426 nm (eqn (1)).

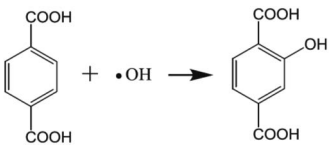

(1)

The samples were suspended in 50 mL of aqueous solution containing 0.05 mol L^{-1} NaOH and 5.0 mmol L^{-1} terephthalic acid. A 350 W UV-light lamp was employed to provide a UV-light source. 5.0 mL of the solution was removed and the TiO_2 was separated from the solution by centrifugation. The remaining clear liquid was used for fluorescence spectrum measurements. The excitation light used to record the fluorescence spectra was 320 nm.[39]

2.2.2. Photocatalytic properties of the dyes. In this work, the photocatalytic properties of the resultant anatase TiO_2 crystal samples were evaluated by photodegradation experiments of three types of dye (50 mg L^{-1}, pH = 3): acid red B (azo), methylene blue (thiazines) and rhodamine B (anthraquinones). A 350 W UV-light lamp was positioned within the central part of the photoreactor and cooling water was circulated through a Pyrex jacket surrounding the photoreactor. A UV-vis absorption spectrophotometer (UV-2500, Shimadzu, Japan) was used to determine the absorbance of the oxidation products. In order to evaluate the degradation efficiency more effectively, we also studied the removal efficiency of COD_{Cr}. COD_{Cr} was determined by the potassium dichromate method.

3. Results and discussion

3.1 Characterization

In this work, in order to explore the effect of triblock copolymers on crystal growth, a comparative experiment was designed. At

the start of this study, the effect of hydrofluoric acid (HF) on crystal facet was investigated and a control experiment for the synthesis of anatase TiO_2 crystals without HF was carried out. As shown in Fig. 1(A1), the representative field emission scanning electron microscopy (FESEM) image shows that the sample was mainly composed of uniform and independent microspheres. The corresponding TEM image (Fig. 1(A2)) reveals a spherical structure of the as-prepared TiO_2 (spherical TiO_2 polycrystalline). Moreover, as shown in Fig. 2(X), a high-magnification FESEM image reveals that the surface of the TiO_2 microspheres is rough and uneven, and that there are no complete (001) facets. In addition, the corresponding EDX spectrum, shown in Fig. 1(A3), indicates that the component elements of the TiO_2 products are Ti and O, where the ratio of atomic number and atomic weight is 1 : 2 and 3 : 2, respectively. However, correspondingly, as shown in Fig. 1(B1) (SEM image) and Fig. 1(B2) (TEM image), anatase TiO_2 single crystals could be synthesized with hydrofluoric acid as a crystal plane controlling agent. From the symmetries of the well-faceted crystal structure of the single crystals, the two flat square surfaces are identified as (001) facets while the other eight isosceles trapezoidal surfaces are (101) facets. Hydrofluoric acid is believed to have dual roles here: (i) to retard hydrolysis of the titanium precursor, and (ii) to reduce the surface energy to promote isotropic growth along the [010] and [100] axes.[39] This result shows that the fluoride ions can effectively reduce the surface energy by Ti–F bonds during the solvothermal synthesis of TiO_2.[42] With the formation of Ti–F bonds, surface O and Ti atoms move inwards and outwards significantly, due to the strong repulsive and attractive interactions of O–F and Ti–F bonds, respectively. A new balance can be established between the O–O/F–O repulsions and Ti–O/Ti–F attractions, which stabilizes the Ti and O atoms on the surfaces.[21,29] Therefore, based on the above mechanism, the (001) facets will be exposed when the crystal grows towards the [010] and [100] axes. The corresponding EDX spectrum, shown in Fig. 1(B3) displays the main elements of the TiO_2 products. Due to the formation of the Ti–F bond, the surface of TiO_2 contains a fluorine element after the synthesis reaction. In the defluorination process, the fluorine atoms on the surfaces of the crystals can easily be removed by heating at 500 °C for 90 min, without changing the crystal structure and morphology.

Focusing on the effects of the triblock copolymers (P123 and F127) on crystal growth, a series of control experiments were designed. As shown in Fig. 2, in the absence of hydrofluoric acid, the resulting spherical TiO_2 microspheres were formed. With an increase in P123, the surface of the spherical TiO_2 polycrystalline becomes increasingly more uniform and regular. As shown in Fig. 2(a1) and (a2), cubic nanocrystals gradually formed on the surface of the spherical polycrystalline under regulation of P123 on the nucleation, growth and self-assembly of TiO_2. Moreover, the size of the cubic nanocrystals on the microspheres was about 60 nm. As is well-known, nanocrystals usually have an agglomeration effect due to the nanoscale effect, and the spherical structure is the most stable and lowest energy form. Therefore, the cubic nanocrystals will agglomerate together in the form of microspheres. In terms of F127, the surface of the spherical TiO_2 polycrystalline becomes smoother with an increase of F127 (Fig. 2(b)). Moreover, it can be seen from Fig. 2 that the morphology of the spherical TiO_2 polycrystalline tends to be of a regular spherical structure with an increase in the triblock copolymers (P123 and F127). The growth process of the spherical TiO_2 polycrystalline is consistent with the principle of minimum energy. In addition, as a surfactant, the triblock copolymers can reduce the surface tension of the material. For the synthesis of the TiO_2 crystals, the surface

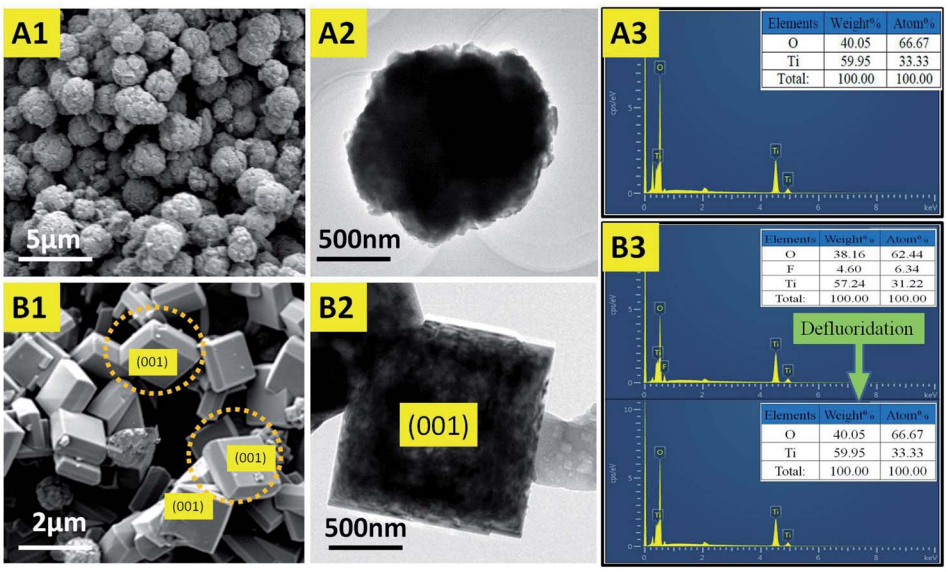

Fig. 1 Microstructures and morphologies of the anatase TiO_2 crystals. (A1) SEM and (A2) TEM images of the typical spherical TiO_2 polycrystalline. (A3) EDX spectrum of the spherical TiO_2 polycrystalline. (B1) SEM and (B2) TEM images of the typical anatase TiO_2 single crystals. (B3) EDX spectrum of the anatase TiO_2 single crystals, before and after defluorination.

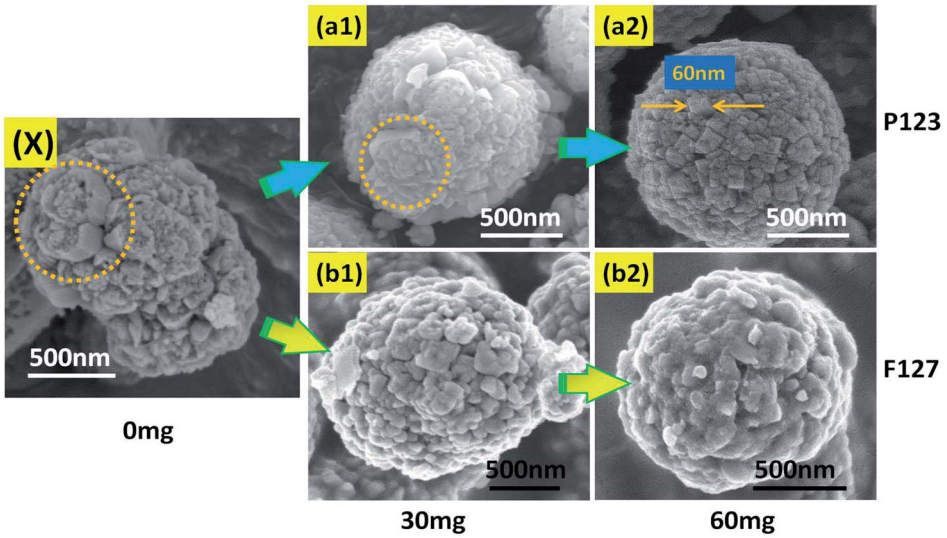

Fig. 2 Microstructures and morphologies of TiO_2 crystals synthesized with different content and type of triblock copolymer (without HF). (X) SEM image of the spherical TiO_2 polycrystalline. P123-spherical TiO_2 polycrystalline at: (a1) 30 mg, (a2) 60 mg. F127-spherical TiO_2 polycrystalline at: (b1) 30 mg, (b2) 60 mg.

tension of the components in the synthetic reaction system will be reduced. Therefore, the TiO_2 crystal tends to be spherical in the growth process.

In contrast, as shown in Fig. 3, anatase TiO_2 crystals with (001) facets could be synthesized with HF as a crystal facet controlling agent. A high-magnification FESEM image (Fig. 3(Y)) reveals that the (001) and (101) facets of TiO_2 single crystals were complete and smooth (truncated octahedron), and that the interfacial angle with a typical value of 68.3° on average was also regular and clear.[21] With the addition of P123, an obvious morphological change was found, as shown in Fig. 3(a1), and that the (001) facets were clearly destroyed. In addition, there was a serious aggregation effect between the crystals. Therefore, the truncated octahedron in the state of mutual adhesion was observed. Moreover, with the increase of P123 (Fig. 3(a2)), the amount of truncated octahedron decreased due to the serious damage to the single crystal, resulting in a large number of irregular fragments of TiO particles. Focusing on F127, the morphology of the TiO_2 crystal clearly changed when F127 was added. As shown in Fig. 3(b1), no truncated octahedron could be seen with serious damage of the single crystal and, with the increase of F127 (Fig. 3(b2)), nanowire clusters appeared around the crystal. Based on the above experimental results, it can be inferred that the triblock

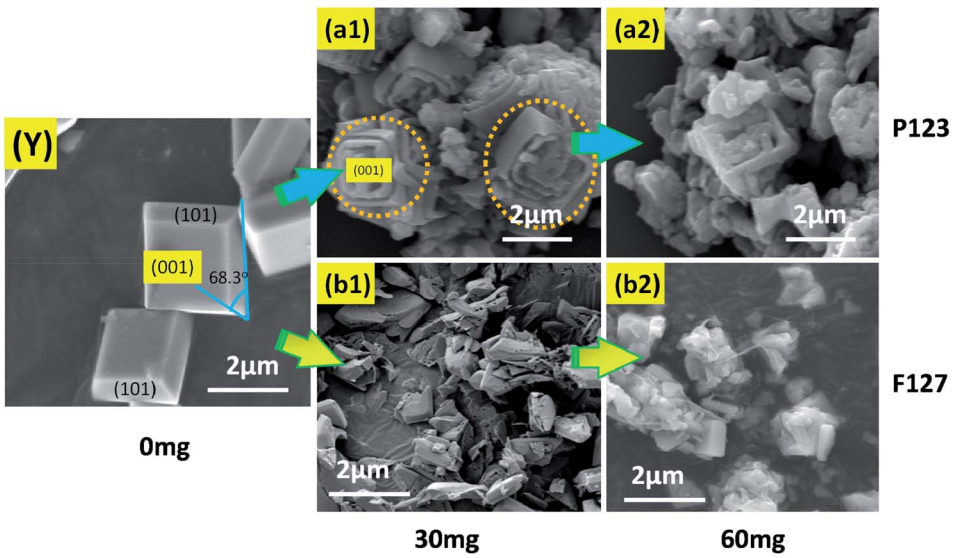

Fig. 3 Microstructures and morphologies of TiO_2 crystals synthesized with different content and type of triblock copolymer (with HF). (Y) SEM image of the anatase TiO_2 single crystals. P123–TiO_2 single crystals at: (a1) 30 mg and (a2) 60 mg. F127–TiO_2 single crystals at: (b1) 30 mg and (b2) 60 mg.

copolymers (P123 and F127) were not conducive to the synthesis of the anatase TiO_2 single crystals.

In order to study the effects of triblock copolymers (P123 and F127) on crystal growth more scientifically, further research on the chemical reactions in the synthesis process was carried out. As shown in Fig. 4, we identified two synthetic routes by analyzing the morphology of anatase TiO_2 single crystals synthesized with different reaction times. As is well-known, HF is crucial for the formation of (001) facets and a truncated octahedron. This is due to the reduction of surface energy and recrystallization of TiO_2 in the presence of a fluorine ion.[21] The possible reactions involved in this process are shown in eqn (2)–(4).

$$TiF_4 + 2H_2O \rightarrow TiO_2 + 4HF \text{ (crystallization)} \quad (2)$$

$$TiO_2 + 6HF \rightarrow H_2TiF_6 + 2H_2O \text{ (dissolution)} \quad (3)$$

$$\left.\begin{array}{l} H_2TiF_6 + 4H_2O \rightarrow Ti(OH)_4 + 6HF \\ Ti(OH)_4 \rightarrow TiO_2 + 2H_2O \end{array}\right\} \text{(recrystallization)} \quad (4)$$

At the beginning of the reaction, the Ti/F ratio is exceedingly high and the rate of crystallization of TiO_2 under hydrothermal conditions is fast (eqn (2)). These crystalline TiO_2 particles aggregate to form a square crystal, which is the route of an anatase TiO_2 single crystal. The free TiO_2 small molecules in the reaction system with a higher surface energy and a smaller diameter dissolve and transfer to the surface of the square crystal, where they redeposit and recrystallize on the better crystallized TiO_2 particles (eqn (3) and (4)). Therefore, under the action of fluorine, the (001) and (101) facets form gradually during the transformation processes of dissolution and recrystallization. However, when P123 is present in the synthesis system, the aggregated TiO_2 crystal with exposed (001) facets was observed after 4 h of the synthesis reaction (Fig. 4(a1)), and the (001) facets were corroded with prolonged synthesis reaction time (Fig. 4(a2) and (a3)). In an acidic environment, the TiO_2 surface is extremely easy to be hydroxylated under hydrothermal conditions. On the crystal surfaces, Ti atoms exist in three states: $TiOH_2^+$, TiO^-, and TiOH. TiOH can be replaced by Ti–F through ligand exchange of the hydroxyl group (–OH) on the crystal surfaces with F ions. With the further replacement of the surface hydroxyl groups, the Ti atoms will eventually be dissolved in the system with the formation of complexes (TiF_6^{2-}). The formation of TiF_6^{2-} leads to the corrosion of the crystal surface. As a surfactant, P123 can accelerate the hydroxylation of the crystal surface by reducing the surface tension of the crystal surface. In terms of the effect of F127 on the TiO_2 single crystal growth, as shown in Fig. 4(b), F127 is clearly not conducive to the formation of the (001) facet or the truncated octahedron. Moreover, the degree of TiO_2 crystal fragmentation increases with prolonged synthesis reaction time. In summary, the triblock copolymers (P123 and F127) are believed to accelerate hydroxylation of the crystal surface in the presence of hydrofluoric acid, and this is not beneficial to TiO_2 single crystal growth.

In this paper, the crystallographic structures of the resultant TiO_2 crystals have been confirmed by X-ray diffraction (XRD), and the diffraction patterns in Fig. 5 clearly indicate that the samples are in the anatase phase (JCPDS card no. 21–1272), with the three most obvious diffraction peaks observed at 25.5° (101), 37.9° (004), and 48.2° (200).[43] This means that the crystal morphology does not affect the crystal phase under certain reaction conditions. Moreover, the diffraction peaks of the anatase TiO_2 single crystals and the P123–TiO_2 single crystals are sharper and more intense compared with those of the F127–TiO_2 single crystals. This is because the crystal structure is destroyed by F127, reducing the crystallinity of the TiO_2 single crystals. The XPS survey spectra of the as-synthesized TiO_2 samples are shown in Fig. 6. It can be seen that the three TiO_2 samples contain only Ti, O and C elements after fluorine has been removed, with sharp photoelectron peaks appearing at binding energies of 458 (Ti 2p), 531 (O 1s) and 285 eV (C 1s). The C 1s peak can be attributed to the adventitious hydrocarbon

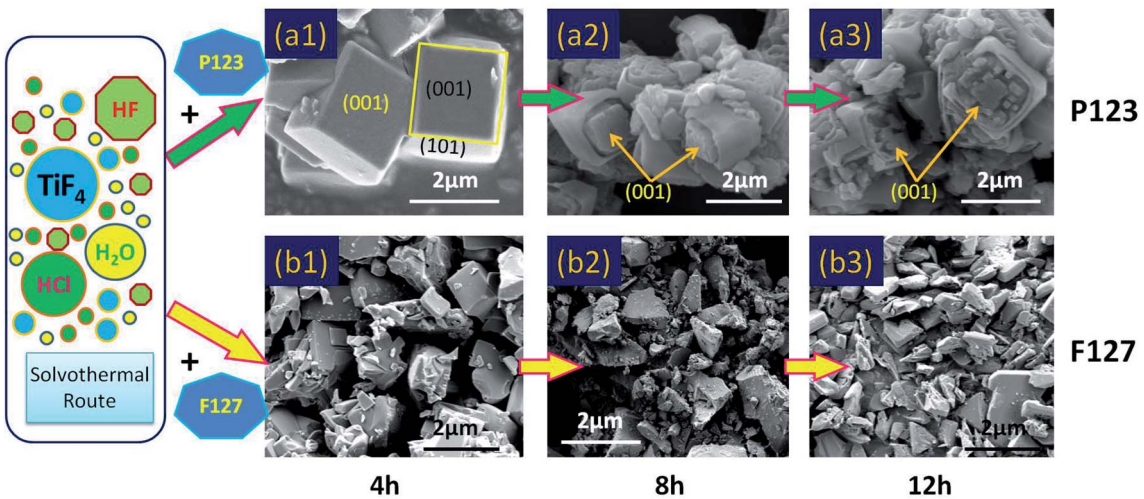

Fig. 4 Morphologies of the anatase TiO_2 single crystals synthesized with different reaction times: 4 h, 8 h and 12 h. (a1)–(a3) with P123 added. (b1)–(b3) with F127 added.

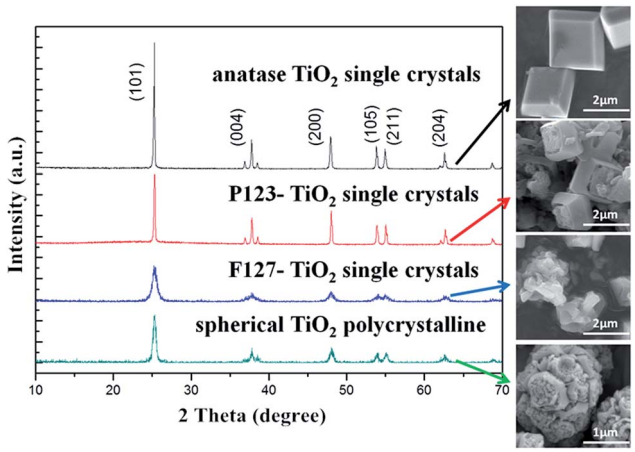

Fig. 5 XRD patterns of the resultant TiO_2 crystal samples.

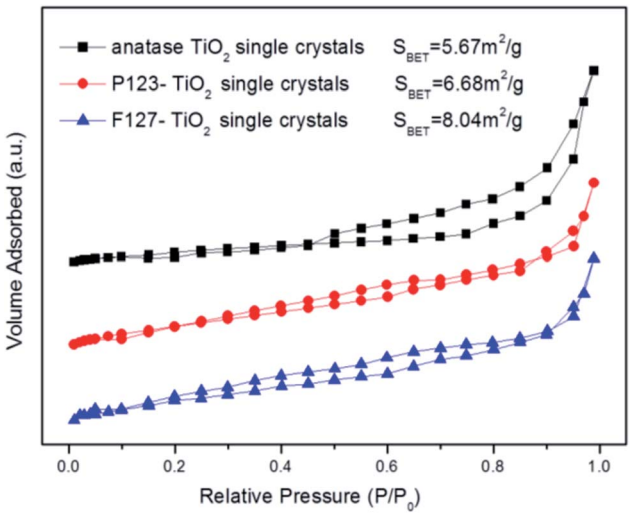

Fig. 7 N_2 adsorption–desorption isotherms of the as-synthesized TiO_2 samples.

from the XPS instrument itself. The N_2 adsorption–desorption isotherms of the three TiO_2 samples are shown in Fig. 7. The adsorption isotherm of the anatase TiO_2 single crystals belongs to the IV and H3 hysteresis loops (IUPAC), suggesting the presence of narrow slit-shaped pores that are generally associated with plate-like particles, and this agrees well with their plate-like morphology. In addition, the existing narrow pores (or the generation of hysteresis loops) are from the aggregation of the single crystals.[44] The adsorption isotherms of the P123–TiO_2 single crystals and F127–TiO_2 single crystals belong to IV and H4 hysteresis loops (IUPAC), suggesting mixed pores of micropores and mesopores. This is mainly due to the accumulation of irregular TiO_2 crystals. Additionally, it can be found that the specific surface areas of the three TiO_2 samples, calculated by the Brunauer–Emmett–Teller (BET) equation, were 5.67 $m^2\ g^{-1}$, 6.68 $m^2\ g^{-1}$ and 8.04 $m^2\ g^{-1}$, respectively.

3.2 Photocatalytic property measurements

For the hydroxyl radical (˙OH) measurements, the capability of forming ˙OHs of anatase TiO_2 single crystals, P123–TiO_2 single crystals and F127–TiO_2 single crystals was examined in this work. As shown in Fig. 8(A), significant fluorescence spectra that are associated with TAOH were generated. The anatase TiO_2 single crystals with complete single crystal morphology and (001) facets could generate more ˙OH with stronger oxidation ability. From the analysis of Fig. 8, we found that the generation of a hydroxyl radical on an anatase TiO_2 single crystal is a short time burst. After 20 minutes of the reaction, the yield of hydroxyl radicals basically reached its peak. The results clearly demonstrate that the completion of the (001) facets is the key to the generation of hydroxyl radicals. Moreover, the normalized concentration of ˙OH generated from anatase TiO_2 single crystals is higher than that of the other two TiO_2 samples. It is also proposed that the simultaneous exposure of the (001) and (101) facets could facilitate charge separation due to the difference in the energy levels of the different crystal facets. The research on the crystal facets found that the conduction band of the (001) facets is slightly higher than that of the (101) facets, calculated by the conduction band and valence band positions of the (001) and (101) facets, thus forming a "surface heterojunction". Therefore, it can be inferred that the anatase TiO_2 single crystals have a complete crystal structure (including (001) and (101) facets), which makes the surface charge move more rapidly and promotes the separation of photoelectron holes.

Due to the results of the hydroxyl radical (˙OH) measurements, it was found that the charge transport will be faster on the surface of the anatase TiO_2 single crystal, and this can help to promote the separation of photogenerated electrons and holes. Therefore, the photocatalytic activity will be greatly improved. Compared with the anatase TiO_2 single crystals, the photocatalytic activities of the P123–TiO_2 single crystals and the F127–TiO_2 single crystals were relatively lower, due to the limitations of their structures. To confirm this, photocatalytic degradation of three types of dye were performed as a probe reaction using these three samples as the photocatalysts.

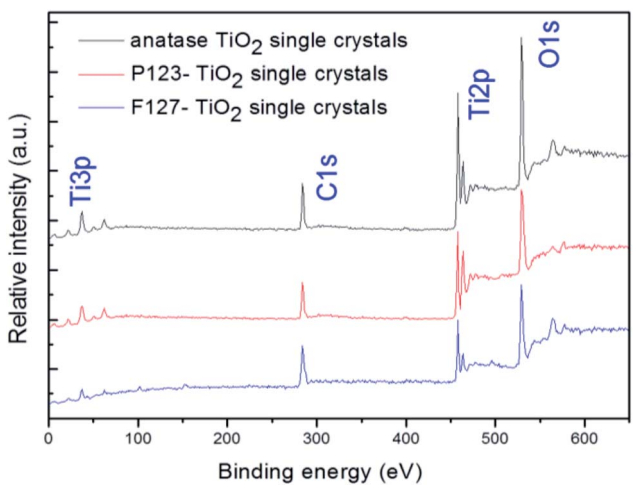

Fig. 6 XPS survey spectra of the as-synthesized TiO_2 samples.

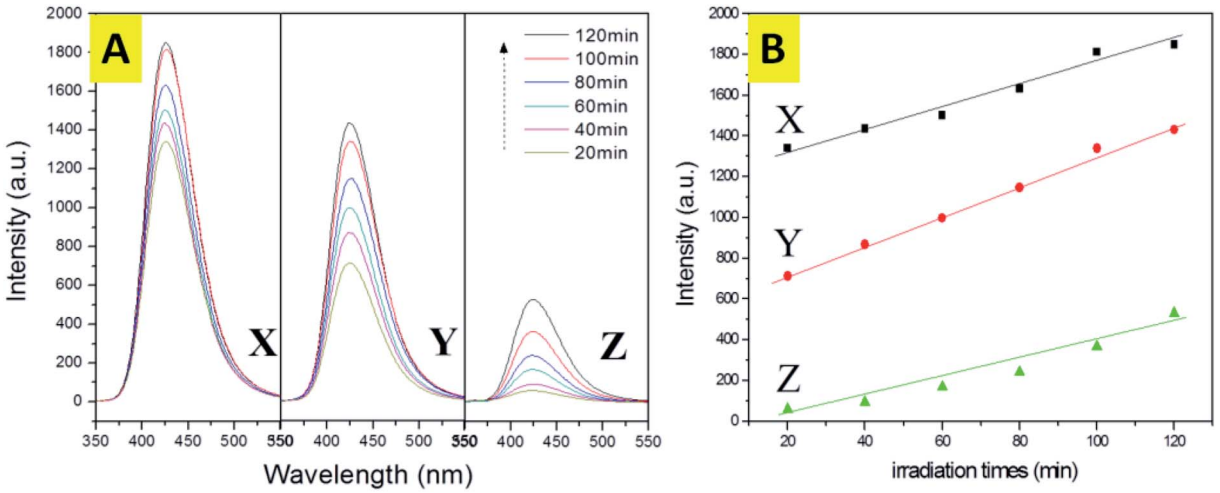

Fig. 8 (A) Fluorescence spectra of terephthalic acid after different irradiation times. (B) Comparison of the photocatalytic oxidation activity with different photocatalysts. (X) Anatase TiO_2 single crystals; (Y) P123–TiO_2 single crystals; (Z) F127–TiO_2 single crystals.

As is well-known from research into the photocatalytic degradation of dyes, the decolorization rate is generally used as the index of the photocatalytic degradation activity. However, the decolorization of a dye only means that its chromophore is destroyed, and does not mean that it is completely mineralized into H_2O and CO_2. In order to evaluate the degradation efficiency of photocatalysis more efficiently, the relationship between the decolorization rate and the COD_{Cr} removal rate was studied. Compared with Fig. 9(A) and (B), the decolorization rate is not equivalent to the COD_{Cr} removal rate. In the process of the photocatalytic degradation of dyes, the removal rate of COD_{Cr} increases with the increase of dye decolorization rate. Fig. 9(A) shows the decolorization efficiency of three types of dye with the anatase TiO_2 single crystals. It can be seen that the anatase TiO_2 single crystals showed remarkably higher efficiency for the photocatalytic degradation of acid red B than for the other two dyes. Similarly, the removal rate of COD_{Cr} of acid red B is also the highest (Fig. 9(B)). These results show that azo dyes are more easily degraded by photocatalysis.

In order to study the photocatalytic activity of the TiO_2 samples on the dyes more scientifically, we conducted a comparative experiment without any TiO_2 (Fig. 10). The results showed that the acid red B (azo) dye is more easily photodissociated under ultraviolet light, leading to decolorization. In the dark reaction process, the decolorization rate of the dyes is proportional to the specific surface area. This is mainly since the larger specific surface area is more conducive to the adsorption of dyes. However, in the process of the photocatalytic reaction, the experimental results showed that the effect of specific surface area on the photocatalytic activity is not decisive. On the contrary, a complete crystal plane structure is the key to the high activity of photocatalysis. Therefore, the anatase TiO_2 single crystals showed remarkably higher efficiencies for the photocatalytic degradation of these three dyes than the other corresponding TiO_2 crystals. This is due to the existence of the (001) and (101) facets that can form an interface effect, which accelerates the transfer rate of photoelectron holes on the crystal surface. Furthermore, it was shown that the photoelectrons of excited TiO_2 tend to move from the (001)

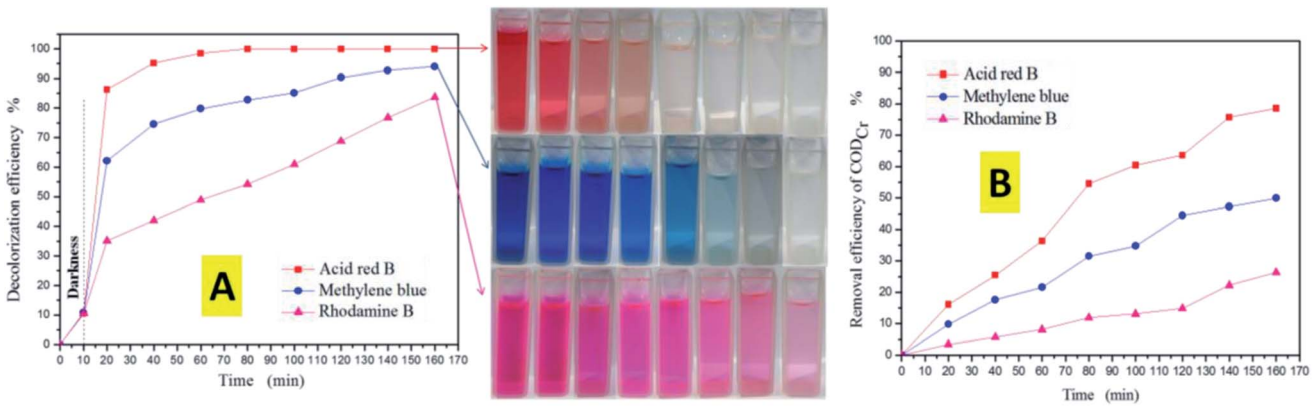

Fig. 9 (A) Decolorization efficiency of the dyes *versus* irradiation time. (B) Removal efficiency of COD_{Cr} *versus* irradiation time.

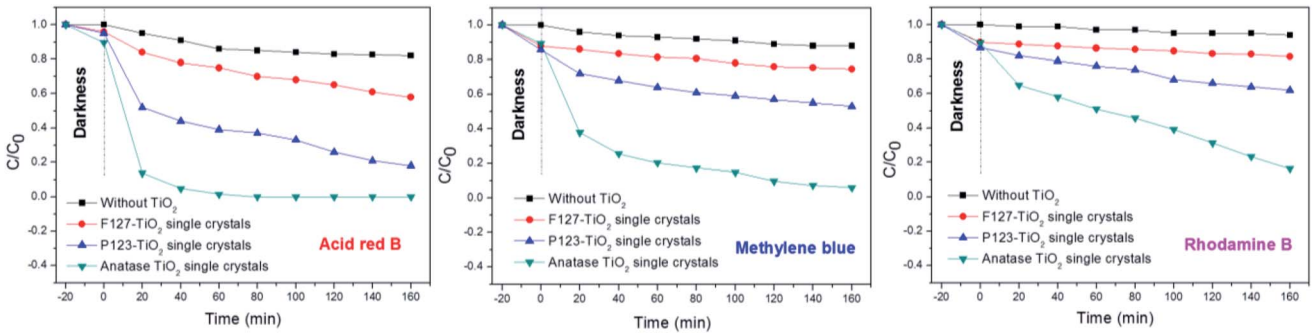

Fig. 10 Comparison of the photocatalytic oxidation activity of dyes with different photocatalysts.

facets to the (101) facets, therefore the accumulation of photogenic holes on the (001) surface will lead to strong oxidation. Significantly, as is shown in the SEM images of the P123–TiO_2 single crystals and F127–TiO_2 single crystals, due to the agglomeration and corrosion of the crystal facets, the photocatalytic activity was severely limited.

4. Conclusions

In this work, the effects of triblock copolymers (P123 and F127) on the growth of TiO_2 crystals were studied. For this purpose, anatase TiO_2 crystals with different morphologies were synthesized by a solvothermal method. Characterization results showed that the triblock copolymers (P123 and F127) can refine the surface structure of the spherical TiO_2 polycrystalline and make the crystal surface homogeneous and smooth. Moreover, P123 can cause the agglomeration effect and hinder the recrystallization process of anatase TiO_2 single crystals, and this will lead to corrosion of the crystal facets. Meanwhile, F127 can destroy crystal formation and hinder the crystal growth due to its special micelle structure. In addition, research on the photocatalytic activity proposed that the integrity of the (001) and (101) facets were critical factors in the photocatalytic reaction. The resultant anatase TiO_2 single crystals could produce more hydroxyl radicals ($^{\bullet}OH$) in the photocatalytic system, which exhibited remarkable photocatalytic performance for the degradation of three types of dye.

Conflict of interest

No potential conflict of interest was reported by the author(s).

References

1 R. G. Li, H. X. Han, F. X. Zhang, D. G. Wang and C. Li, *Energy Environ. Sci.*, 2014, **7**, 1369–1376.
2 B. Wang, L. Si, J. Geng, Y. Su, Y. Li, X. Yan and L. Chen, *Appl. Catal., B*, 2017, **204**, 316–323.
3 Z. W. Gao, W. F. Jin, Y. P. Li, Q. J. Song, Y. L. Wang, K. Zhang, S. Wang and L. Dai, *J. Mater. Chem. C*, 2015, **3**, 4511–4514.
4 H. Guo, R. Gao, M. Sun, H. Guo, B. Wang and L. Chen, *Chemsuschem*, 2019, **12**, 487–494.
5 B. K. Sunkara and R. D. K. Misra, *Acta Biomater.*, 2008, **4**, 273–283.
6 R. M. Ali, M. R. Elkatory and H. A. Hamad, *Fuel*, 2020, **268**, 117297.
7 G. Sui, J. Li, L. Du, Y. Zhuang, Y. Zhang, Y. Zou and B. Li, *J. Alloys Compd.*, 2020, **823**, 153851.
8 M. Pastore, T. Etienne and F. De Angelis, *J. Mater. Chem. C*, 2016, **4**, 4346–4373.
9 M. Diak, E. Grabowska and A. Zaleska, *Appl. Surf. Sci.*, 2015, **347**, 275–285.
10 X. H. Lu, G. M. Wang, T. Zhai, M. H. Yu, J. Y. Gan, Y. X. Tong and Y. Li, *Nano Lett.*, 2012, **12**, 1690–1696.
11 D. Depan and R. D. K. Misra, *Mater. Sci. Eng., C*, 2014, **34**, 221–228.
12 X. G. Han, X. Wang, S. F. Xie, Q. Kuang, J. J. Ouyang, Z. X. Xie and L. S. Zheng, *RSC Adv.*, 2012, **2**, 3251–3253.
13 I. Garcia-Fernandez, I. Fernandez-Calderero, M. I. Polo-Lopez and P. Fernandez-Ibanez, *Catal. Today*, 2015, **240**, 30–38.
14 S. Jia, J. Li, G. Sui, L. Du, Y. Zhang, Y. Zhuang and B. Li, *RSC Adv.*, 2019, **9**, 31177–31185.
15 D. Gao, W. Liu, Y. Xu, P. Wang, J. Fan and H. Yu, *Appl. Catal., B*, 2020, **260**, 118190.
16 L. Pan, M. Ai, C. Huang, L. Yin, X. Liu, R. Zhang, S. Wang, Z. Jiang, X. Zhang, J.-J. Zou and W. Mi, *Nat. Commun.*, 2020, **11**, 418.
17 P.-Y. Hsieh, Y.-H. Chiu, T.-H. Lai, M.-J. Fang, Y.-T. Wang and Y.-J. Hsu, *ACS Appl. Mater. Interfaces*, 2019, **11**, 3006–3015.
18 T. M. David, P. Wilson, R. Mahesh, P. Sagayaraj, N. Murugesan, C. Ramesh and H. Seshadri, *Mater. Technol.*, 2018, **33**, 288–300.
19 X. Q. Gong and A. Selloni, *J. Phys. Chem. B*, 2005, **109**, 19560–19562.
20 Q. J. Xiang, K. L. Lv and J. G. Yu, *Appl. Catal., B*, 2010, **96**, 557–564.
21 H. G. Yang, C. H. Sun, S. Z. Qiao, J. Zou, G. Liu, S. C. Smith, H. M. Cheng and G. Q. Lu, *Nature*, 2008, **453**, 638–641.
22 Y. Dong and X. Fei, *Mater. Technol.*, 2020, **35**, 102–111.
23 E. J. W. Crossland, N. Noel, V. Sivaram, T. Leijtens, J. A. Alexander-Webber and H. J. Snaith, *Nature*, 2013, **495**, 215–219.

24 Y. Q. Dai, C. M. Cobley, J. Zeng, Y. M. Sun and Y. N. Xia, *Nano Lett.*, 2009, **9**, 2455–2459.
25 J. D. Peng, H. H. Lin, C. T. Lee, C. M. Tseng, V. Suryanarayanan, R. Vittal and K. C. Ho, *RSC Adv.*, 2016, **6**, 14178–14191.
26 J. Liu, P. Wang, J. Fan and H. Yu, *J. Energy Chem.*, 2020, **51**, 253–261.
27 Y. Dong and F. Meng, *RSC Adv.*, 2020, **10**, 12511–12518.
28 W. Jiao, Y. P. Xie, R. Z. Chen, C. Zhen, G. Liu, X. L. Ma and H. M. Cheng, *Chem. Commun.*, 2013, **49**, 11770–11772.
29 M. G. Xu, P. Ruan, H. X. Xie, A. Yu and X. F. Zhou, *ACS Sustainable Chem. Eng.*, 2014, **2**, 621–628.
30 P. Fu, Y. Ma, G. Li and X. Lin, *RSC Adv.*, 2019, **9**, 38381–38390.
31 D. Nguyen, W. Wang, H. B. Long, W. J. Shan, X. D. Li, M. Fang, M. Y. Li, X. Q. Wang and H. Q. Ru, *Microporous Mesoporous Mater.*, 2016, **230**, 177–187.
32 Y. Huang, J. Ho, Z. Wang, P. Nakashima, A. J. Hill and H. T. Wang, *Microporous Mesoporous Mater.*, 2009, **117**, 490–496.
33 E. L. Crepaldi, G. J. D. A. Soler-Illia, D. Grosso, F. Cagnol, F. Ribot and C. Sanchez, *J. Am. Chem. Soc.*, 2003, **125**, 9770–9786.
34 W. Wang, D. Nguyen, H. B. Long, G. Q. Liu, S. Li, X. Y. Yue and H. Q. Ru, *J. Mater. Chem. A*, 2014, **2**, 15912–15920.
35 Y. X. Yang, F. Su, S. Q. Zhang, W. Guo, X. Yuan and Y. H. Guo, *Colloids Surf., A*, 2012, **415**, 399–405.
36 L. Peng, Y. W. Liu, S. H. Gao, X. M. Chen, P. Xin, X. H. Dai and B. J. Ni, *Sci. Rep.*, 2015, **5**, 12331.
37 H. Miyata, Y. Fukushima, Y. Kanno, S. Hayase, S. Hara, M. Watanabe, S. Kitamura, M. Takahashi and K. Kuroda, *J. Mater. Chem. C*, 2015, **3**, 3869–3875.
38 Z. M. Liu, L. Peng and A. W. Tang, *Chin. Chem. Lett.*, 2016, **27**, 1801–1804.
39 Y. Dong, X. Fei, Z. Liu, Y. Zhou and L. Cao, *Appl. Surf. Sci.*, 2017, **394**, 386–393.
40 Y. F. Li, D. H. Xu, J. I. Oh, W. Shen, X. Li and Y. Yu, *ACS Catal.*, 2012, **2**, 391–398.
41 Y. J. Wang, Y. M. He, T. T. Li, J. Cai, M. F. Luo and L. H. Zhao, *Chem. Eng. J.*, 2012, **189**, 473–481.
42 C. K. Nguyen, H. G. Cha and Y. S. Kang, *Cryst. Growth Des.*, 2011, **11**, 3947–3953.
43 H. G. Yang, G. Liu, S. Z. Qiao, C. H. Sun, Y. G. Jin, S. C. Smith, J. Zou, H. M. Cheng and G. Q. Lu, *J. Am. Chem. Soc.*, 2009, **131**, 4078–4083.
44 Z. Y. Wang, K. L. Lv, G. H. Wang, K. J. Deng and D. G. Tang, *Appl. Catal., B*, 2010, **100**, 378–385.

